Gap plasmon-polariton nanoresonators: Scattering enhancement and launching of surface plasmon polaritons

Jesper Jung* and Thomas Søndergaard
Department of Physics and Nanotechnology, Aalborg University, Skjernvej 4A, DK-9220 Aalborg Øst, Denmark

Sergey I. Bozhevolnyi
Institute of Sensors, Signals and Electrotechnics (SENSE), University of Southern Denmark, Niels Bohrs Allé 1, DK-5230 Odense M, Denmark

(Received 10 June 2008; revised manuscript received 12 August 2008; published 5 January 2009)

Gap plasmon-polariton (GPP) nanoresonators based on a metal nanostrip separated with a small gap from a metal surface or metal block are considered. Scattering resonances and field enhancements are studied for two-dimensional structures using the Green's-function surface integral equation method (GFSIEM). For small gaps, we show that the scattering resonances occur due to the constructive interference of counterpropagating GPPs, forming standing waves. By varying the gap size we find that the resonance wavelength can be tuned over a wide range of wavelengths, which makes the resonators interesting for spectroscopic and sensing applications, and observe the transition between GPP-based resonators (for narrow gaps) and slow surface plasmon-polariton (SPP) strip resonators (for wide gaps). Considering the resonant field distributions, we find that, for an insulator thickness of 10 nm, the maximum field enhancement (with respect to the incident field) can reach values close to 50 along the line passing through the gap center. For the case of a strip placed close to a metal surface, two scattering channels, viz., the out-of-plane scattering and the scattering into SPPs (propagating along the surface) are evaluated separately using a generalized version of the GFSIEM. We find that, even though the out-of-plane scattering is in general dominating in the considered range of parameters, scattering into SPPs can be very efficient for smaller gaps featuring a cross section that at resonance even exceeds the strip width. The considered properties of GPP nanoresonators, i.e., resonant scattering and local-field enhancements along with efficient scattering into SPPs, hold promises for their useful applications within plasmonic sensing devices.

DOI: 10.1103/PhysRevB.79.035401 PACS number(s): 78.67.−n, 71.36.+c, 73.20.Mf, 02.70.Pt

I. INTRODUCTION

Metallic nanorods, nanowires, and nanostrips have recently attracted a great deal of attention in the design of optical resonators and optical antennas[1–23] because they show strong resonant enhancement in light scattering or extinction and also because of the possibility of strong electromagnetic field-enhancement effects in the near-field region of the structures. Especially gaps between adjacent metal nanostructures allow for very high fields and localization of light way beyond the diffraction limit.[2,16–18,22,23] These properties make metallic nanostructures interesting for sensing and spectroscopic purposes.[24]

Composite metal nanostructures support super plasmon-polariton (PP) modes, which in some cases can become more localized and more strongly bound than regular surface plasmon polaritons (SPPs).[25,26] An example of such a highly localized PP mode is the gap plasmon-polariton (GPP) mode between two metal surfaces. In this paper, we are particularly interested in what happens when a metal strip is placed close to a metal surface. In such a configuration a GPP mode can be formed in the gap, and similar to resonances of metal strips and slow SPP strip modes,[14,15,20] scattering resonances of the strip-surface configuration can be related to the GPP mode. We analyze two different configurations: one where the metal surface is of finite width (a metal block) and one where the width of the metal surface is infinite, configurations (a) and (b), respectively (Fig. 1). Coherent presentation of these configurations, showing also the link to (individual) nanostrip resonators,[14,15] is one of the goals of this paper. Another goal is to consider the usage of configuration (b), where light can be scattered both out of the surface plane and into SPPs that propagate along the surface, for launching of SPPs. The directional (left and right) SPP excitation is evaluated using the generalized version of the Green's-function surface integral equation method (GFSIEM) we presented in Ref. 27.

In the latter context, it should be noted that scattering into SPPs is a subject of great interest in plasmonics, and many different configurations have been considered for local SPP

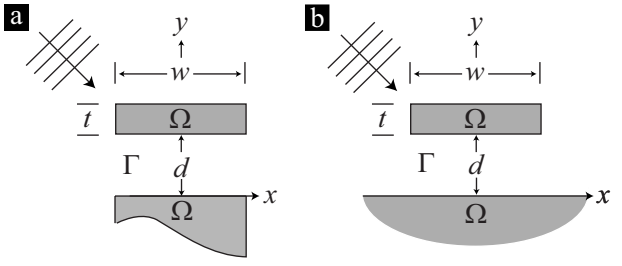

FIG. 1. The two GPP resonators analyzed. (a) A plane wave propagating in the xy plane is scattered by a lossy metal strip of thickness t and width w placed at a distance d from a lossy metal surface of width w. The metals are surrounded by Γ, a lossless dielectric medium. (b) The situation is the same as in (a) except for the width of the surface, which is infinite.

excitation, e.g., SPP launching through an array of nanoholes,[28] through a subwavelength slit supplemented with a periodic set of grooves[29] or by a surface protrusion defect in the form of a particle or a single ridge,[30] as well as by a periodic set of those.[31] The efficiency of SPP excitation for some configurations has been evaluated both experimentally and numerically.[31,32] A very recent study of SPP excitation by a single subwavelength hole in a gold film[32] revealed an efficiency of up to 28%. Note though that this is the value normalized with respect to the power incident onto the hole area, implying that the corresponding scattering (into SPPs) cross section is smaller than one-third of the hole area.

This paper is organized as follows. In Sec. II, the resonator structures and the theoretical method used in the numerical analysis are presented. Section III presents the results. We start with a brief discussion of the GPP mode. Hereafter we present the numerical analysis of the two GPP-based nanoresonator configurations (Sec. III A and Sec. III B, respectively). This is followed by the conclusion in Sec. IV.

II. STRUCTURES AND METHOD

A. Structures

The GPP resonators that we investigate consist of lossy metals Ω surrounded by lossless dielectrics Γ (Fig. 1). The optical properties of the metals are characterized by a complex-frequency-dependent dielectric constant ε_Ω, and the dielectric is characterized by a real-frequency-independent dielectric constant ε_Γ. The problem is reduced to two dimensions by considering both the structure and fields invariant under translation along the z axis, which is out of the paper. The situation that we analyze is the scattering of a monochromatic p-polarized plane wave propagating in the xy plane. p polarization is chosen because plasmons are p polarized. Two different GPP-based resonator configurations are analyzed (Fig. 1).

In configuration (a), a plane wave is scattered by a metal strip of thickness t and width w placed at a distance d from a metal surface of width w. In configuration (b), the width of the metal surface is infinite.

B. Method

The numerical analysis of the two configurations (Fig. 1) is performed using the GFSIEM which is an appropriate and efficient method for the analysis of two-dimensional scattering problems in open infinite domains.[27,33,34] This is primarily because the GFSIEM only involves integrals over the boundary of the scatterers as the radiating boundary conditions are satisfied through an appropriate choice of Green's function and, secondarily, because the GFSIEM allows for a good description of the metal surfaces. The latter is important since we are particularly interested in SPPs and GPPs, which have field maxima at the metal surfaces. As we consider p polarization $[\mathbf{H}(\mathbf{r})=H(\mathbf{r})\hat{z}]$ it is convenient to formulate the surface integral equations by means of the magnetic field as this yields scalar equations. The standard scalar surface integral equations for the magnetic field read as[33,34]

$$H(\mathbf{r}) = H_0(\mathbf{r}) + \oint_{\partial\Omega} [H(\mathbf{s}')\hat{n}' \cdot \nabla' g_\Gamma(\mathbf{r},\mathbf{s}') - g_\Gamma(\mathbf{r},\mathbf{s}')\hat{n}' \cdot \nabla' H_\Gamma(\mathbf{s}')]dl' \quad \text{for} \quad \mathbf{r} \in \Gamma, \tag{1a}$$

$$H(\mathbf{r}) = -\oint_{\partial\Omega} \left[H(\mathbf{s}')\hat{n}' \cdot \nabla' g_\Omega(\mathbf{r},\mathbf{s}') - g_\Omega(\mathbf{r},\mathbf{s}')\frac{\varepsilon_\Omega}{\varepsilon_\Gamma}\hat{n}' \cdot \nabla' H_\Gamma(\mathbf{s}') \right] dl' \quad \text{for} \quad \mathbf{r} \in \Omega, \tag{1b}$$

where $H_0(\mathbf{r})$ is the incident field, $\mathbf{s}'$ is a point on the boundary of Ω, $\hat{n}$ is the outward normal of Ω, $\partial\Omega$ is the boundary of Ω, and the boundary condition $\hat{n}' \cdot \nabla' H_\Omega(\mathbf{s}') = \varepsilon_\Omega/\varepsilon_\Gamma \hat{n}' \cdot \nabla' H_\Gamma(\mathbf{s}')$ has been used, where H_Γ and H_Ω refer to the magnetic field approaching the boundary from medium Γ and Ω, respectively, and the Green's functions $g_{\Gamma,\Omega}(\mathbf{r},\mathbf{s}')$ are given by the zero-order Hankel function of second kind $g_{\Gamma,\Omega}(\mathbf{r},\mathbf{s}') = H_0^{(2)}(k_0\sqrt{\varepsilon_{\Gamma,\Omega}}|\mathbf{r}-\mathbf{s}'|)/(4i)$, where k_0 is the vacuum wave number.

Configuration (b) [Fig. 1(b)] is, however, not suitable for the standard GFSIEM [Eq. (1)] because the boundary of Ω is infinite, and one would have to integrate along this infinite boundary. In configuration (a) this can very simply be avoided by assuming that the lower metal has a finite thickness. If the thickness of the lower metal is much larger than the skin depth of the electromagnetic field, this assumption is very good. Configuration (b) is, however, much more difficult to handle because even though a finite thickness of the metal surface is assumed the boundary is still infinite. In order to work around this problem, we developed a generalized version of the GFSIEM,[27] where the integral along the infinite surface is omitted by the use of an appropriate Green's function outside of the metal strip. Using this method an exact numerical analysis of configuration (b) can be made without truncations of integrals or assumptions of finite structures. The tradeoff is that the Green's function used outside the metal strip cannot be represented by means of a simple Hankel function but must be evaluated by means of more complicated, numerically difficult, and computationally time-consuming Sommerfeld integrals. For further details we refer to Ref. 27.

III. RESULTS

In all calculations presented, the optical properties of the dielectric regions Γ are described using the refractive index of quartz $n_\Gamma = 1.452$. The metal chosen is silver as it is known from previously presented results[14,17,23] that strong plasmon resonances occur in related geometries based on silver. The dielectric constant of silver is obtained by linear interpolation of the data in Ref. 35. In all calculations sharp corners have been rounded with a radius of curvature of 2 nm for numerical reasons.

Our physical interpretation of the scattering resonances of the configurations [(a) and (b), Fig. 1] is in the following section related to the GPP mode supported by a gap sand-

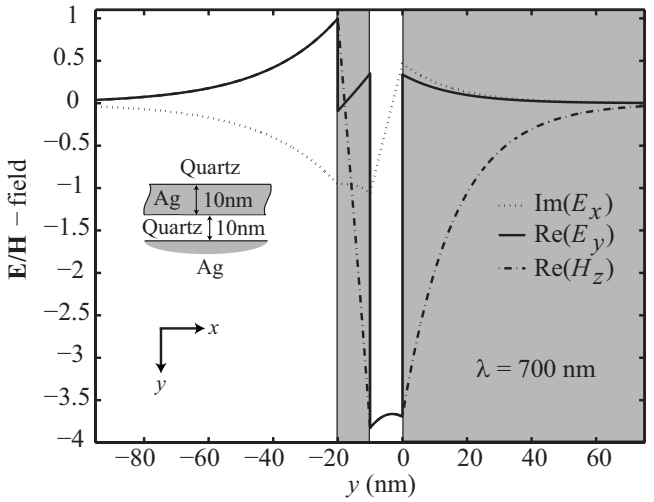

FIG. 2. The distribution of the components of the electric and the magnetic fields of the GPP mode supported by a 10 nm quartz gap sandwiched between a silver half plane and a thin silver film of 10 nm thickness, for $\lambda=700$ nm. According to the coordinate system chosen, the direction of propagation of the GPP wave is along the x axis and the field distributions are displayed along the y axis (see inset).

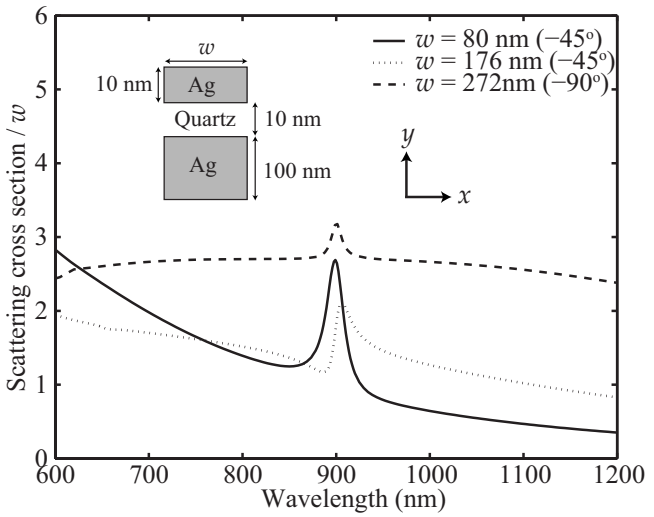

FIG. 3. The scattering cross section versus free space wavelength for configuration (a). A plane wave propagating at an angle (relative to x) axis indicated in the legend is scattered by the structure [$t=10$ nm, $d=10$ nm, and $t_2=100$ nm (see inset)]. Three different widths w are considered.

wiched between a thin metal film and a metal surface (Fig. 2). It is seen how the GPP mode is characterized by a large electric field in the gap and how the field decays exponentially away from the structure in the direction transverse to the propagation direction, which is along the x axis (see inset of Fig. 2).

To justify the assumption of a finite thickness of the lower metal block in configuration (a) we have investigated the dependence of the mode index of the GPP mode on the thickness of the lower metal block. We find that for thicknesses larger than ~50 nm the mode index is practically constant. In all scattering calculations performed on configuration (a) a thickness of $t_2=100$ nm is used for the lower metal block.

Also, the dependence of the mode index of the GPP mode versus the gap size has been investigated. Two distinct regimes were observed: for small gaps (below ~50 nm), the mode index decreases for an increasing gap size, and for larger gaps, the mode index becomes constant. Interestingly, for large gaps (above ~200 nm) the mode index of the GPP mode converges toward the mode index of the slow SPP strip mode. This indicates that the GPP mode for wide gaps transforms into a slow SPP strip mode and therefore becomes decoupled from the lower surface.

A. Configuration (a)

In the analysis of configuration (a), we start by relating the scattering resonances to the GPP mode. Even though the width of the metals is finite, the GPP mode can still propagate along the x axis, and because the GPP is strongly bound to the gap, it will be efficiently reflected when it reaches the end of the resonator. Similar to the case of symmetric nanostrip configurations,[14,17,22] constructive interference between forward- and backward-propagating GPPs can give rise to standing-wave resonances at certain wavelengths, which will show up in the scattering spectrum.

To demonstrate this, we have calculated the scattering cross section for three different widths, which corresponds to first, second, and third order resonances at the wavelength $\lambda_0=900$ nm, respectively (Fig. 3). The configuration with $w=80$ nm has a first-order resonance at $\lambda_0=900$ nm. The real part of the mode index of the GPP mode supported by the configuration is $n_{GPP}=4.69$, which yields $\lambda_{GPP}/2 \approx 96$ nm. It is known that if the width of the resonator is increased by half the wavelength of the PP mode responsible for the resonance, a one-order higher resonance will be positioned at approximately the same wavelength.[14,17,22] Thus a resonator with $w=176$ nm should have a second-order resonance around $\lambda_0=900$ nm, and a resonator with $w=272$ nm should have a third-order resonance. For the third-order resonance, the angle of incidence has been changed to −90°. This has been done in order to better reveal the scattering peak from the spectrum. This angle (−90°) cannot be used to excite the second-order resonance due to symmetry mismatch between the incident field and the resonance field. The field patterns in Fig. 4 clearly illustrate the third, second, and first-order natures of the GPP resonance for the different widths. In (a) three minima of the field are seen in the gap, in (b) two, and in (c) one. The field patterns show how the mode field, at resonance, is highly localized in the gap. From (d)–(f) the standing-wave pattern of the field is clearly seen.

With sensing and spectroscopical applications in mind, an important feature of resonant nanostructures is tunability of the resonance wavelength. It is known that the resonance wavelength is a strong function of the gap size in related configurations.[7–10,18] To investigate the tunability of the resonance wavelength, and furthermore to study the transition from a GPP resonator to a slow SPP strip resonator, we have calculated the scattering cross section of a monochromatic plane wave scattered at an angle of −45° (with respect to the

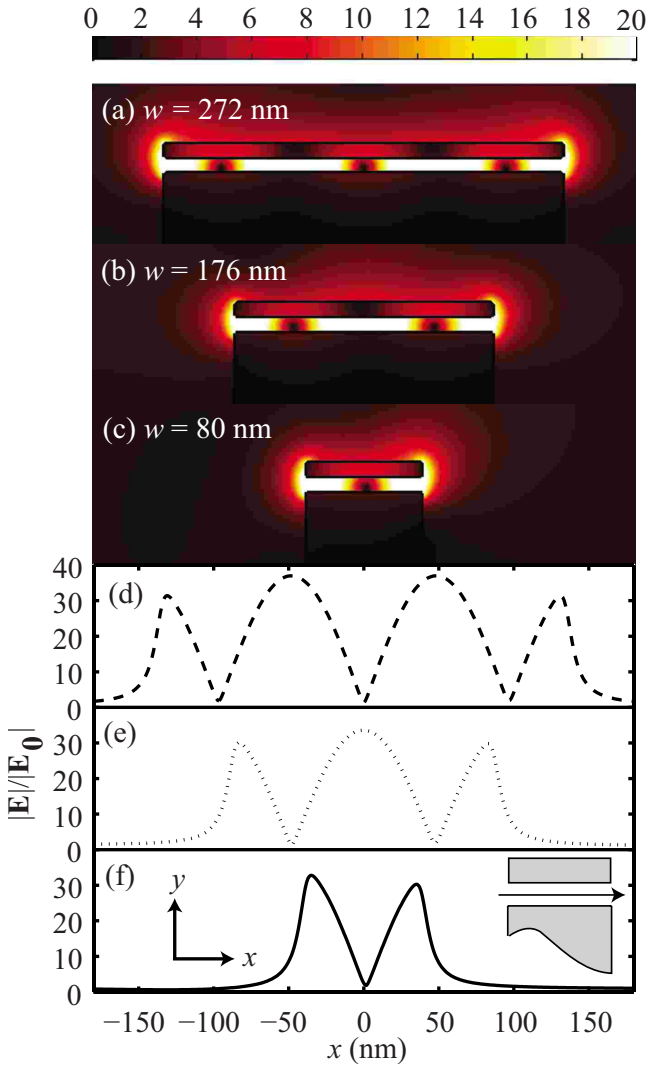

FIG. 4. (Color online) Electric-field magnitude in the xy plane for three different resonator widths: (a) $w=272$ nm, (b) $w=176$ nm, and (c) $w=80$ nm [$t=10$ nm, $d=10$ nm, and $t_2=100$ nm (see inset of Fig. 3)]. Cross-sectional plot of the electric-field magnitude (parallel to the x axis) through the center of the gap [see inset in (f)]. (d) $w=272$ nm, (e) $w=176$ nm, and (f) $w=80$ nm. All field plots have been calculated at the resonance wavelength $\lambda_0=900$ nm.

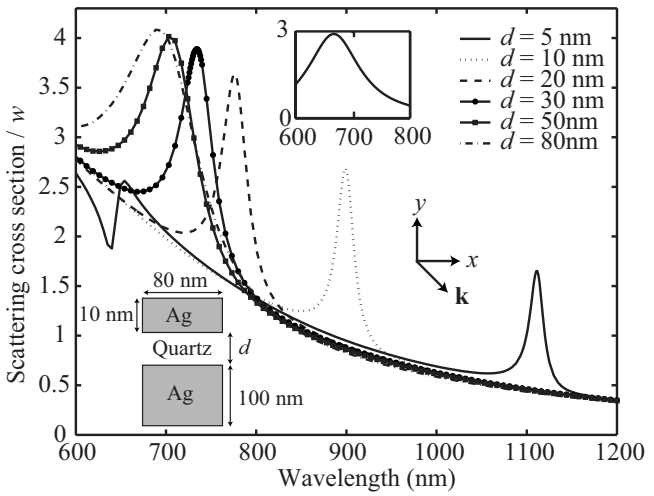

FIG. 5. Scattering cross section versus wavelength for a monochromatic plane wave propagating at an angle of −45° with respect to the x axis scattered of configuration (a) [$t=10$ nm, $w=80$ nm, and $t_2=100$ nm (see inset)]. Six different gap sizes have been considered. The second inset depicts the scattering cross section versus wavelength of a strip resonator [$t=10$ nm and $w=80$ nm] surrounded by quartz.

x axis) by configuration (a) for varying gap sizes (Fig. 5). It is seen that the resonance wavelength is a strong function of the gap size, and by changing the gap size from 80 to 5 nm, the resonance wavelength is redshifted more than 400 nm, from 690 to 1110 nm. The resonance shift is far from linear with the gap size. For small gaps it is shifted much more than for larger gaps, e.g., λ_0 shifts more than 200 nanometers (from 900 to 1110 nm) when the gap size is reduced by only 5 nm, from 10 to 5 nm, and it shifts only 15 nm (from 690 to 705 nm) when the gap size is reduced by 30 nm, from 80 to 50 nm. This behavior is in good agreement with our interpretation of the resonances as a smaller gap results in a larger GPP mode index and thus a larger GPP wavelength.

Another expectation from the investigation of the GPP mode is that when the gap size becomes large, the resonator no longer resembles a GPP resonator but instead acts as a slow SPP strip resonator. The second inset in Fig. 5 shows the scattering cross section versus wavelength for a single strip resonator [$t=10$ nm and $w=80$ nm] surrounded by quartz. This scattering peak is similar to the scattering peak of configuration (a) for $d=80$ nm. The resonance wavelength of the strip resonator is $\lambda_0=665$ nm, and the resonance wavelength of configuration (a) for $d=80$ nm is 690 nm. This illustrates that configuration (a) for $d=80$ nm is relatively close in resembling a strip resonator. However, it must be noted that a large increase in gap size is needed to blueshift the resonance wavelength the last 25 nm as for gap sizes above 80 nm the resonance wavelength dependence on the gap size is weak. To further study the transition from a GPP resonator to a slow SPP strip resonator in configuration (a), and to study field-enhancement effects in the gap, we have calculated the electric-field magnitude in the xy plane for different gap sizes (Fig. 6). The electric-field magnitude for a gap size of $d=10$ nm [Fig. 4(c)] shows that the field is highly concentrated in the gap. The field is large, close to the terminations of the resonator, and has a clear minimum close to the center of the gap. The reason that the minimum is not completely in the center of the gap is that the angle of incidence is −45°. From the cross-sectional plot through the center of the gap [Fig. 4(f)] a maximum field enhancement, with respect to the incident field, above 30 is found. A higher value is possible with the angle of incidence −90°, where a maximum enhancement of 49 is found for $d=10$ nm and $w=80$ nm. For $d=30$ nm, at resonance ($\lambda_0=734$ nm), most of the characteristics of the GPP mode are still found in the field pattern [Fig. 6(a)]; the mode still has a tendency of being connected to the lower metal surface through the gap. However, the largest field is no longer found in the gap but rather at the terminations of the strip. From the cross-

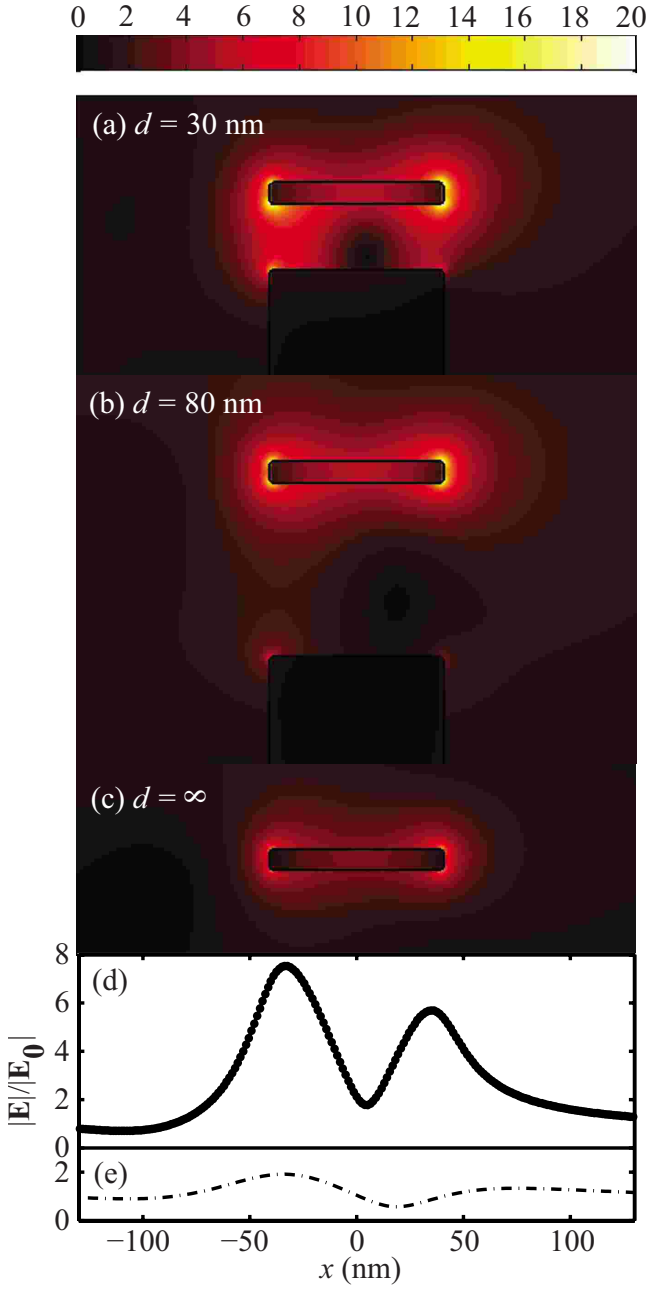

FIG. 6. (Color online) Electric-field magnitude in the xy plane for different gap sizes [$t=10$ nm, $w=80$ nm, and $t_2=100$ nm (see inset of Fig. 5)]. (a) $d=30$ nm and $\lambda_0=734$ nm, (b) $d=80$ nm and $\lambda_0=690$ nm, and (c) $d=\infty$ and $\lambda_0=665$ nm. Cross-sectional plot of the electric-field magnitude parallel to the x axis through the center of the gap. (d) $d=30$ nm and (e) $d=80$ nm.

sectional plot through the center of the gap [Fig. 6(d)] the maximum field enhancement is also considerably lower than for $d=10$ nm, approximately 7.5 which is at least four times smaller. For $d=80$ nm [Figs. 6(b) and 6(e)], the field mostly resembles a metal strip resonator [Fig. 6(c)], where the field is confined to the strip and not in the gap. For $d=80$ nm, the maximum field enhancement through the center of the gap is below 2 [Fig. 6(e)].

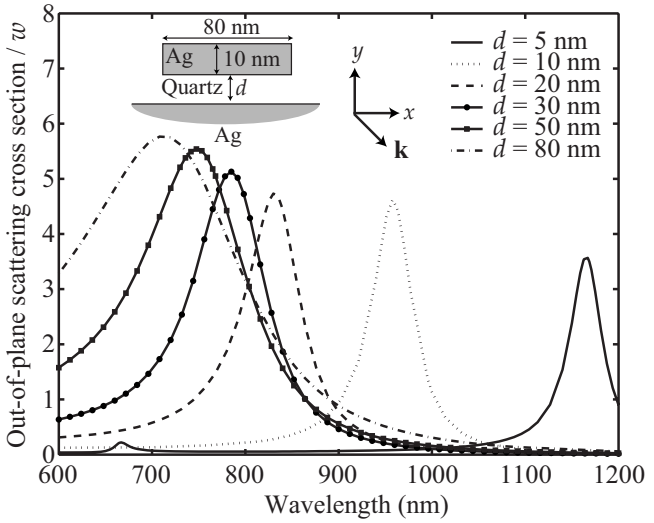

FIG. 7. The out-of-plane scattering cross section versus wavelength. A plane wave propagating at an angle of −45° (with respect to the x axis) is scattered by configuration (b) [$t=10$ nm, $w=80$ nm, and for six values of d (see inset and legend)].

B. Configuration (b)

Using the method we presented in Ref. 27, we have calculated the scattering cross sections of the two main scattering channels of configuration (b), viz., the out-of-plane scattering (Fig. 7) and scattering into SPPs (Fig. 8). All the same tendencies as in the scattering analysis of configuration (a) (Fig. 5) are seen. When the gap size is decreased the resonance wavelength is redshifted. However, when compared to configuration (a), a larger redshift is seen, the resonance peaks are broader, and also larger values of the peak maxima are seen. That the resonances of configuration (b) are redshifted compared to configuration (a) is in good agreement with our interpretation of them. Due to the infinite surface, the terminations of the resonator in configuration (b) are less sharp than in configuration (a). This makes the effective length of the resonator in configuration (b) larger than in configuration (a), and the resonances therefore get redshifted. More rapid coupling of energy out of the resonator, in this case both into out-of-plane propagating waves (the peak values in Fig. 7 are higher than in Fig. 5) and SPPs, results in broadening of the scattering peaks. The SPP scattering cross section is calculated as an integral of the time averaged flux of the Poynting vector of the scattered field related to SPPs. Due to losses in the metal, SPPs are damped as they propagate along the surface, and thus the SPP scattering cross section is a function of the distance that the SPPs have propagated as

$$\sigma_{\mathrm{SPP}}(x) = A_{\mathrm{SPP}} \exp(-2\,\mathrm{Im}(k_{\mathrm{SPP}})|x|), \tag{2}$$

where A_{SPP} is a constant, k_{SPP} is the SPP wave number, and $|x|$ is related to the distance that the SPPs have propagated along the x axis. In order to compare the amount of light scattered into SPPs to the out-of-plane propagating waves, x should be chosen to be small and close to the resonator. In the results presented (Fig. 8) we have chosen $|x|=1000$ nm, where $x=0$ is in the center of the strip. When the SPP scat-

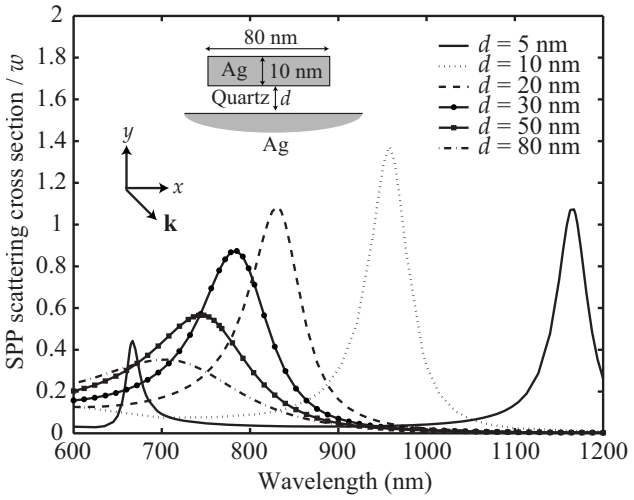

FIG. 8. The SPP scattering cross section versus wavelength. See caption of Fig. 7 for details.

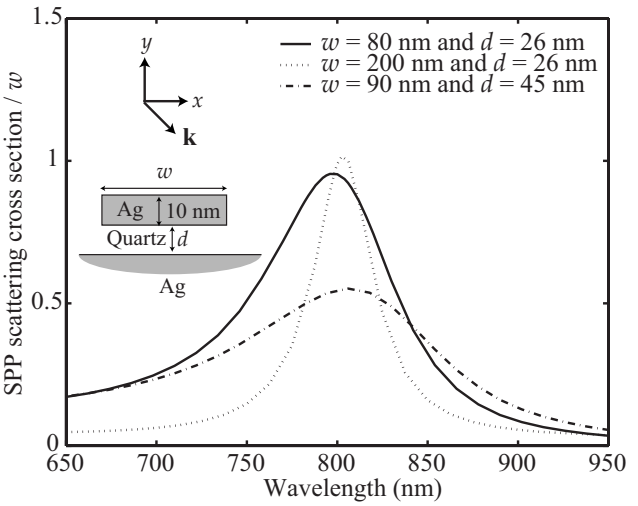

FIG. 9. The SPP scattering cross section versus wavelength for silver strips of different width, where the gap is adjusted such that a resonant launching of SPPs is achieved around a free space wavelength of $\lambda_0 = 800$ nm. For details of configurations see inset and legends.

tering is compared to the out-of-plane scattering, it is seen that the resonance wavelengths are, within a few nanometers, identical. However, the SPP scattering cross section is smaller. The SPP scattering cross section increases when the gap size is reduced and has a maximum around a gap size of 10 nm, with a value close to 1.4. This is about 30% of the out-of-plane scattering cross section which is close to 5. For comparison, in a very recent study of SPP excitation by a single subwavelength hole in a gold film,[32] the highest efficiency achieved (normalized with respect to the power incident onto the hole area) was below 30%, implying that the normalized scattering (into SPPs) cross section was below 0.3. The close to fivefold increase in the efficiency predicted for the 10-nm-wide gap structure is related to the occurrence of strong resonance in the scattering configuration (Fig. 8) that enhances not only local but also scattered fields.

To demonstrate structure optimization of configuration (b) with respect to SPP launching, we have calculated a series of SPP scattering cross sections in which the strip width and gap are adjusted such that the structures show resonant launching of SPPs around a free space wavelength of 800 nm (Fig. 9). The calculations show how it is possible to achieve resonant SPP launching at a desired wavelength by carefully playing with the structural parameters (in Fig. 9 the width of the strip and the gap size) of configuration (b). Note that both first- (e.g., $w=80$ nm and $d=26$ nm) and second- ($w=200$ nm, $d=26$ nm, and $\lambda_{GPP}/2 \approx 120$ nm) order resonances can be utilized for resonant launching of SPPs. It should also be taken into consideration that, in terms of the absolute efficiency of SPP excitation, the second-order resonance shown in Fig. 9 ensures a 2.5-fold efficiency increase when compared to the first-order one.

With development of plasmonic devices in mind, a strong unidirectional coupling into SPPs is often favorable.[36] In order to investigate the directionality of the launched SPPs of configuration (b) under oblique incidence, we have calculated two SPP scattering cross sections related to SPPs that propagate in the negative (to the left) and positive (to the right) x directions (Fig. 10). It is seen how the SPP scattering cross section of SPPs that propagate to the left is blueshifted a few nanometers compared to the scattering cross section of SPPs that propagate to the right. At resonance, however, the strength of the two scattering cross sections are almost identical. Thus, even under oblique incidence (−45° with respect to the x axis), SPPs that propagate along the surface are launched with almost equal strength in both directions. However, this is expected as scattering into SPPs is related to the occurrence of the strong resonant buildup of the standing waves in the gap, and these standing waves are only slightly asymmetric [see field calculations for configuration (b) presented in Fig. 11].

To investigate the transition from GPP resonator to SPP strip resonator, and to study the field enhancement in the gap, we have calculated the field for three different gap sizes for

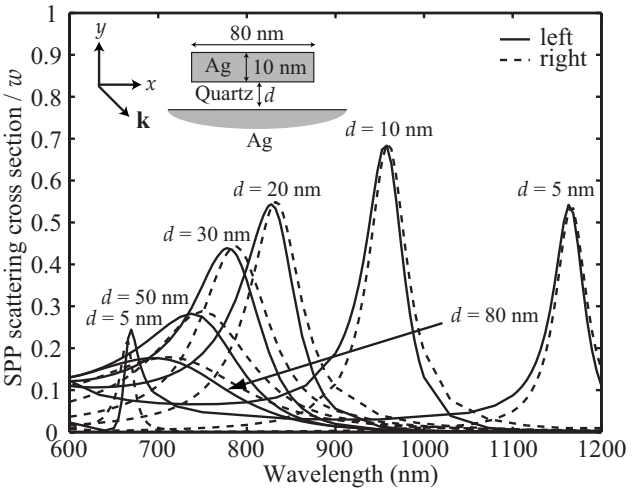

FIG. 10. The SPP scattering cross section versus wavelength. The solid lines represent the scattering cross section of SPPs that propagate to the left and the dashed lines SPPs that propagate to the right. See caption of Fig. 7 and inset for details about the configuration.

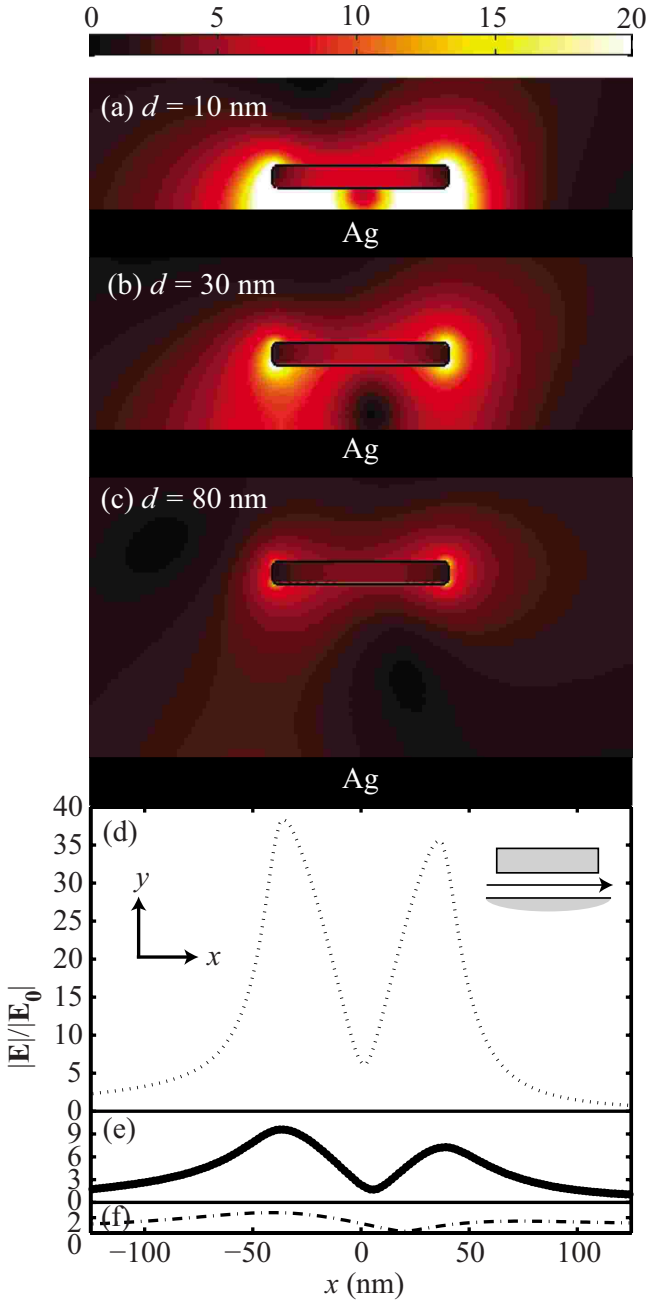

FIG. 11. (Color online) Electric-field magnitude at resonance in the xy plane of configuration (b) ($t=10$ nm, $w=80$ nm, and three different gap sizes). A plane wave is incident at an angle of $-45°$ with respect to the x axis. (a) $d=10$ nm and $\lambda_0=958$ nm. (b) $d=30$ nm and $\lambda_0=785$ nm. (c) $d=80$ nm and $\lambda_0=712$ nm. Cross sectional plots of the field magnitude through the center of the gap along the x axis. (d) $d=10$ nm, (e) $d=30$ nm, and (f) $d=80$ nm.

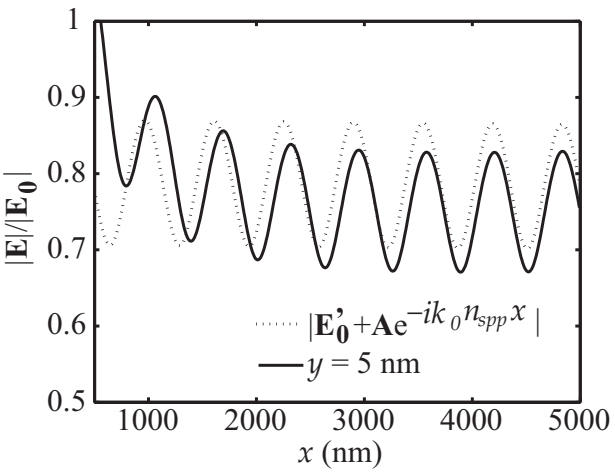

FIG. 12. A cut along the x axis of the magnitude of the electric field at $y=5$ nm. The cut is shown at resonance $\lambda_0=958$ nm for the configuration $t=d=10$ nm, $w=80$ nm, and an angle of incidence of $-90°$. Also shown is $|\mathbf{E}_0'+\mathbf{A}\exp(-ik_0 n_{\mathrm{SPP}}x)|$, where $\mathbf{E}_0'$ is the incident field including its reflection from the surface and $\mathbf{A}$ is the amplitude vector of the SPP electric field.

configuration (b) (Fig. 11). When compared to the fields of configuration (a) (Fig. 6), the fields in the gaps are slightly increased. The maximum field enhancement in the gap ($d=10$ nm) is close to 40 [Fig. 11(d)], and again a higher value can be obtained for the angle of incidence of $-90°$. In this case the maximum value is 48. Also, the modes at resonance in configuration (b) are wider than in configuration (a). This makes the effective resonator width larger, which makes sense, as argued above. In configuration (b) the field for $d=80$ nm is, as in configuration (a), mostly localized around the strip and not within the gap. Thus for a gap size of $d=80$ nm, the field of configuration (b) also mostly resembles the field of a strip resonator.

In order to reveal the launched SPPs that propagate along the silver surface from the near-field plots, a cut along the x axis at $y=5$ nm of the electric-field magnitude is presented together with $|\mathbf{E}_0'+\mathbf{A}\exp(-ik_0 n_{\mathrm{SPP}}x)|$, where $\mathbf{E}_0'$ is the incident field including its reflection from the surface and $\mathbf{A}$ is the amplitude vector of the SPP electric field, determined using Eqs. (27)–(29) of Ref. 27 (Fig. 12). As the two curves are quite similar, it is seen how the characteristics of the electric-field magnitude are mainly dominated by the interference between $\mathbf{E}_0'$ and the SPP that propagates along the surface. The reason that the two curves deviate slightly is that the electric-field magnitude also contains propagating scattered waves.

From the above analysis of configuration (b) it is clear that the scattering resonances of both resonator configurations [(a) and (b)] have a common origin. The resonances in the scattering spectra are due to constructive interference of counterpropagating GPPs that are trapped in the quartz gap below the strip. For certain wavelengths these form standing-wave resonances. As the terminations of the resonator in configuration (b) are weaker than in (a), the resonances of (b) are broader and redshifted.

IV. CONCLUSION

In conclusion, we have, using the GFSIEM, theoretically analyzed two GPP resonator configurations, viz., a metal strip close to a metal block of finite width [configuration (a)] and a metal strip close to an infinitely wide metal surface [configuration (b)]. We have shown that the scattering resonances of both configurations (a) and (b) have a common origin and can be related to the GPP mode supported by the

gap between the strip and the block/surface. As the GPP mode is efficiently reflected at the resonator terminations due to its strongly bound nature, standing-wave patterns can form from constructive interference between forward- and backward-propagating GPPs, which gives rise to the scattering resonances. As the terminations of the resonator in configuration (b) are less sharp, the scattering resonances are redshifted and broader than in configuration (a). We have shown how the scattering resonance wavelength can be tuned over a wide range of frequencies from the upper visible to the near infrared by varying the gap size of the configurations. For wide gaps, we have established a link between gap and strip resonators, as the two GPP resonator configurations for wide gaps clearly resemble slow SPP strip resonators. Also field-enhancement effects in the gap of the two configurations were analyzed. The largest field enhancement in the gap was found in configuration (b). For a gap size of 10 nm a field enhancement close to 40, with respect to the incident field, was found for a nonoptimized angle of incidence. For an optimized angle of incidence a value close to 50 was found in both configurations. Finally, noticing that in configuration (b) there appears the possibility of exciting SPPs, we have considered the efficiency of this process. We were able to evaluate scattering into out-of-plane propagating waves and into SPPs separately and found that for a gap size of 10 nm scattering into SPPs is about 30% of the out-of-plane scattering. The considered properties of the GPP resonators make them attractive for use within plasmonic sensing devices.

ACKNOWLEDGMENTS

The authors (J.J., T.S., and S.B.) gratefully acknowledge the financial support from the NABIIT project financed by the Danish Research Agency (Contract No. 2106-05-033), (T.S.) from the Danish Research Council for Technology and Production, and (S.B.) from the European Network of Excellence, PLASMO-NANO-DEVICES (Contract No. FP6-2002-IST-1-507879).

*jung@nano.aau.dk

[1] H. Ditlbacher, A. Hohenau, D. Wagner, U. Kreibig, M. Rogers, F. Hofer, F. R. Aussenegg, and J. R. Krenn, Phys. Rev. Lett. **95**, 257403 (2005).
[2] P. Mühlschlegel, H. J. Eisler, O. J. F. Martin, B. Hecht, and D. W. Pohl, Science **308**, 1607 (2005).
[3] K. Imura, T. Nagahara, and H. Okamoto, J. Chem. Phys. **122**, 154701 (2005).
[4] H. T. Miyazaki and Y. Kurokawa, Phys. Rev. Lett. **96**, 097401 (2006).
[5] F. Neubrech, T. Kolb, R. Lovrincic, G. Fahsold, A. Pucci, J. Aizpurua, T. W. Cornelius, M. E. Toimil-Molares, R. Neumann, and S. Karim, Appl. Phys. Lett. **89**, 253104 (2006).
[6] T. Laroche and C. Girard, Appl. Phys. Lett. **89**, 233119 (2006).
[7] G. Lèvêque and O. J. F. Martin, Opt. Lett. **31**, 2750 (2006).
[8] G. Lèvêque and O. J. F. Martin, Opt. Express **14**, 9971 (2006).
[9] A. Christ, T. Zentgraf, S. G. Tikhodeev, N. A. Gippius, O. J. F. Martin, J. Kuhl, and H. Giessen, Phys. Status Solidi B **243**, 2344 (2006).
[10] A. Christ, T. Zentgraf, S. G. Tikhodeev, N. A. Gippius, J. Kuhl, and H. Giessen, Phys. Rev. B **74**, 155435 (2006).
[11] L. Novotny, Phys. Rev. Lett. **98**, 266802 (2007).
[12] Y. Kurokawa and H. T. Miyazaki, Phys. Rev. B **75**, 035411 (2007).
[13] O. L. Muskens, V. Giannini, J. A. Sánchez-Gil, and J. G. Rivas, Opt. Express **15**, 17736 (2007).
[14] T. Søndergaard and S. I. Bozhevolnyi, Phys. Rev. B **75**, 073402 (2007).
[15] T. Søndergaard and S. I. Bozhevolnyi, Opt. Express **15**, 4198 (2007).
[16] S. I. Bozhevolnyi and T. Søndergaard, Opt. Express **15**, 10869 (2007).
[17] T. Søndergaard and S. I. Bozhevolnyi, Phys. Status Solidi B **245**, 9 (2008).
[18] A. Christ, G. Lèvêque, O. J. F. Martin, T. Zentgraf, J. Kuhl, C. Bauer, H. Giessen, and S. G. Tikhodeev, J. Microsc. **229**, 344 (2008).
[19] G. A. Wurtz, W. Dickson, D. O'Connor, R. Atkinson, W. Hendren, P. Evans, R. Pollard, and A. V. Zayats, Opt. Express **16**, 7460 (2008).
[20] T. Søndergaard, J. Beermann, A. Boltasseva, and S. I. Bozhevolnyi, Phys. Rev. B **77**, 115420 (2008).
[21] G. Della Valle, T. Søndergaard, and S. I. Bozhevolnyi, Opt. Express **16**, 6867 (2008).
[22] T. Søndergaard, J. Jung, S. I. Bozhevolnyi, and G. Della Valle, New J. Phys. **10**, 105008 (2008).
[23] J. Jung and T. Søndergaard, Proc. SPIE **6988**, 69881N (2008).
[24] S. Lal, S. Link, and N. J. Halas, Nat. Photonics **1**, 641 (2007).
[25] H. Raether, *Surface Plasmons-on Smooth and Rough Surfaces and on Gratings*, 1st ed. (Springer-Verlag, Berlin, 1988).
[26] W. L. Barnes, A. Dereux, and T. W. Ebbesen, Nature (London) **424**, 824 (2003).
[27] J. Jung and T. Søndergaard, Phys. Rev. B **77**, 245310 (2008).
[28] E. Devaux, T. W. Ebbesen, J.-C. Weeber, and A. Dereux, Appl. Phys. Lett. **83**, 4936 (2003).
[29] F. López-Tejeira, S. G. Rodrigo, L. Martín-Moreno, F. J. García-Vidal, E. Devaux, J. Dintinger, T. W. Ebbesen, J. R. Krenn, I. P. Radko, and S. I. Bozhevolnyi, New J. Phys. **10**, 033035 (2008).
[30] H. Ditlbacher, J. R. Krenn, N. Felidj, B. Lamprecht, G. Schider, M. Salerno, A. Leitner, and F. R. Aussenegg, Appl. Phys. Lett. **80**, 404 (2002).
[31] H. Ditlbacher, J. R. Krenn, A. Hohenau, A. Leitner, and F. R. Aussenegg, Appl. Phys. Lett. **83**, 3665 (2003).
[32] A.-L. Baudrion, F. de León-Pérez, O. Mahboub, A. Hohenau, H. Ditlbacher, F. J. García-Vidal, J. Dintinger, T. W. Ebbesen, L. Martín-Moreno, and J. R. Krenn, Opt. Express **16**, 3420 (2008).
[33] J. Jin, *The Finite Element Method in Electromagnetics*, 2nd ed. (Wiley, New York, 2002).
[34] T. Søndergaard, Phys. Status Solidi B **244**, 3448 (2007).
[35] E. Palik, *Handbook of Optical Constants of Solids*, 1st ed. (Academic, U.S., 1985).
[36] F. López-Tejeira *et al.*, Nat. Phys. **3**, 324 (2007).